Time domain-based gear contact fatigue analysis of a wind turbine drivetrain under dynamic conditions

Wenbin Dong [a,*], Yihan Xing [a], Torgeir Moan [a,b], Zhen Gao [a]

[a] Centre for Ships and Ocean Structures (CeSOS), Norwegian University of Science and Technology (NTNU), Otto Nielsens V.10, N-7491 Trondheim, Norway
[b] Department of Marine Technology, Norwegian University of Science and Technology (NTNU), Otto Nielsens V.10, N-7491 Trondheim, Norway

ARTICLE INFO

Article history:
Received 4 June 2012
Received in revised form 25 October 2012
Accepted 29 October 2012
Available online 6 November 2012

Keywords:
Contact fatigue
Gears
Wind turbine
Time domain
Weibull

ABSTRACT

This paper presents a general approach to predict the contact fatigue life of the gears in the drive-train system of a wind turbine under dynamic conditions. A simplified predictive pitting model that estimates service lives is presented and validated by comparisons with published experimental evidence. Finally, the predictive model is used to estimate the contact fatigue lives of the sun gear and planetary gears in the drive-train system of the National Renewable Energy Laboratory's 750 kW land-based wind turbine based on time domain simulations. The occurrence frequencies of different wind speeds are described by the generalized gamma distribution. The time series of the torques in the main shaft are obtained from a global dynamic response analysis of the wind turbine. The time series of the gear contact forces is obtained from a dynamic analysis of the gearbox using multi-body simulation. The two-parameter Weibull distribution, the three-parameter Weibull distribution, and the generalized-gamma distribution are used to fit the long-term probabilistic distribution of the gear tooth contact pressures. The case study shows the validity of the approach presented in this paper.

1. Introduction

The gearbox is one of the most expensive components of the wind turbine system and has experienced higher-than-expected failure rates since the inception of the wind energy industry [1]. The load prediction, design, fabrication, and operation of gearboxes have been improved over the past two decades using internationally recognized gearbox wind turbine design standards [2] produced by close collaboration between wind turbine manufactures, gear designers, bearing manufacturers, consultants, and lubrication engineers. To increase the long-term reliability of gearboxes, there has been increasing interest in developing techniques that utilize time domain simulations to predict gearbox design loads.

In addition, modern industries (e.g., the wind energy industry) commonly require that mechanical elements (e.g., wheels, gears, bearings, and cams) be designed to carry high loads at high speeds with minimum size and weight. Reliable prediction of operational failures of components in such applications is the key issue in ensuring an adequate design. In the case of gears, two prominent modes of fatigue damage have been identified: (i) tooth root bending fatigue and (ii) contact fatigue (often called surface pitting). These modes of damage are considered in international standards such as AGMA [3], DIN [4] and ISO 6336 [5]. Gear tooth pitting may initiate at defects such as dents or scratches on the surface (surface initiated) or by near-surface plastic deformation in the region of maximum cyclical shear stress caused by cyclic rolling–sliding contact (subsurface initiated). The former is usually observed in gears with rough surfaces and poor lubrication. The latter, which is common in gears with smooth contact surfaces and good lubrication [6], is addressed in this study because it is characteristic of surface pitting in high quality gear mechanisms. Pitting studies date back to the experiments of Way [7]. Different models and methods have been applied to pitting analyses of gears in recent years. Coy et al. [8] applied the Lundberg–Palmgren model [9] to analyze the dynamic capacity and surface fatigue life of spur and helical gears. Keer et al. [10,11] analyzed subsurface and surface cracking due to Hertzian contact and suggested a pitting model for rolling contact fatigue using a half-space condition, Hertzian stress theory and the body force method in conjunction with a Paris law (2D fracture mechanics). Murakami et al. [12] analyzed surface crack propagation on a lubricated rolling contact using the body force method in conjunction with finite element analysis. Hanson and Keer [13] developed a three-dimensional analytical model for the crack propagation phase of the surface pitting failure process. Mow and Cheng [14] analyzed the thermal stresses in an elastic half-space associated with an arbitrarily distributed moving heat source. Goshima and Hanson [15] performed a three-dimensional analysis of thermal effects on surface crack

propagation on rolling contacts. Glodez et al. [6,16,17] performed a series of comprehensive studies on contact fatigue of gears using dislocation motion theory, short crack theory and the maximum tangential stress (MTS) criterion. Fajdiga et al. [18] investigated the influence of different parameters on surface pitting of contacting mechanical elements using elasto–hydrodynamic lubrication conditions and the virtual crack extension method in conjunction with finite element analysis. Osman and Velex [19] recently studied the possible interactions between contact fatigue and dynamic tooth loads on gears.

However, the vast majority of the studies on gears have not considered the influence of environmental loading conditions on the occurrence of gear tooth surface failures in the gearbox of the drive-train system of a wind turbine using time domain simulations. This is mainly due to two limitations (i) lack of a suitable simplified gear contact fatigue prediction model and (ii) lack of a fully coupled analysis of the global dynamic response of the wind turbine and the dynamics of the internal drive-train. The purpose of this paper is to present a general approach to perform time domain-based gear contact fatigue analysis of the drive-train system of a wind turbine under dynamic conditions that links a global dynamic response analysis of the wind turbine with a detailed contact fatigue analysis of gears in the drive-train. The main idea is to investigate how the long-term distribution of gear contact pressures can be represented by analytical functions such as the Weibull distribution and the generalized gamma distribution, which are necessary for probabilistic reliability analyses of gears using probabilistic approaches and to develop simplified methods for practical design. The National Renewable Energy Laboratory's 750 kW land-based Gearbox Reliability Collaborative wind turbine is used as a case study. The global aero-elastic simulations of the wind turbine are performed using the FAST code from NREL [20]. The time series of the main shaft torques are obtained and used as inputs in a multibody gearbox model in SIMPACK [21]. A simplified predictive pitting model to estimate service lives is presented and validated by comparisons with published experimental evidence. A linear elastic fracture mechanics (LEFMs) model is used to predict the number of cycles of crack propagation. The two-parameter Weibull distribution, the three-parameter Weibull distribution and the generalized-gamma distribution are used to fit the long-term probabilistic distribution of the gear tooth contact pressures.

2. Predictive models to estimate service lives

2.1. Crack initiation

The initiation of fatigue cracks represents the first stage of the pitting process. The periods mainly depend on different combinations of rolling and sliding contact conditions (surface roughness, surface damage, lubrication), which can vary widely. The maximum stress that leads to crack initiation can be either on or under the surface [22]. For single crystal materials, the crack initiation stage can make up a major part of the fatigue life, and failure occurs almost instantaneously thereafter. For polycrystalline materials that are commonly used for gears, many possible stress concentrations, due to grain boundaries, crystal voids, triple points, or inclusions, may separately, or in combination initiate a sub-surface crack almost immediately upon load application [16]. In several previous studies, Mura and Nakasone [23] provided an analytical model based on the theory of dislocation motion on persistent slip bands, which can be used to describe the changes in the material's microstructure due to an applied load and to determine the number of stress cycles required to initiate a fatigue crack. Glodez et al. [24] and Fajdiga and Sraml [25] used the strain-life method with the finite element method (FEM) to determine the number of stress cycles required to initiate a fatigue crack caused by bending fatigue in a gear tooth root and contact fatigue of gear teeth flanks, respectively. Osman and Velex [19] applied Crossland's criterion, Liu-Zenner's criterion and Dang Van's criterion to predict the number of stress cycles required for fatigue crack initiation due to contact fatigue of gear teeth flanks under cyclic dynamic conditions. In general, the contribution of crack initiation to the total contact fatigue life of gear teeth flanks is limited and predictions have large uncertainties. Therefore, the number of stress cycles required for crack initiation is neglected in this study.

2.2. Deterministic model for crack propagation

2.2.1. Linear elastic fracture mechanics model

The prediction of crack propagation requires a proper estimate of the crack initiation point and the crack propagation rate. Linear elastic fracture mechanics concepts have been used to estimate the crack propagation rate in several previous studies, [19,26–29]. The driving force for subsurface crack propagation in rolling contacts and shown experimentally depend on the hardness and the maximum shear stress [27,30]. Hence, the micro-hardness and maximum shear stress distribution are incorporated into the prediction model for crack propagation. Based on the Paris–Erdogans equation, the following linear elastic fracture mechanics model is used to describe crack propagation:

$$\frac{da}{dN} = C \cdot (\Delta K)^m \tag{1}$$

where a is the half-length of the crack, N is the number of loading cycles, C and m are the material constants, and ΔK is the stress intensity factor range.

2.2.2. Stress intensity factor calculation

In 1985, Hearle and Johnson [31] developed a mode II stress intensity factor model and calculated the mode II stress intensity factors at each end of a crack in a half-space where the stress field over the whole crack is known. Choi and Liu [29,32] used this model to estimate the contact fatigue life of bearings and compared it with experimental results. The model is given as follows:

$$\Delta K_{II} = \sqrt{\frac{2}{\pi \cdot 2a}} \int_0^{2a} \tau_c(x_{2a} - \xi) \cdot \left\{ \frac{2a - \xi}{\xi} \right\}^{1/2} d\xi \tag{2}$$

Where τ_c represents the net shear stress, which is the stress available to cause the stress intensities at the crack tip. The meanings of other parameters used in Eq. (2) are shown in Fig. 1 [29].

Accordingly, the following equivalent shear stress, $\tau_{eqv.}$, is assumed to be the net shear stress based on the aforementioned findings [19,27,30]:

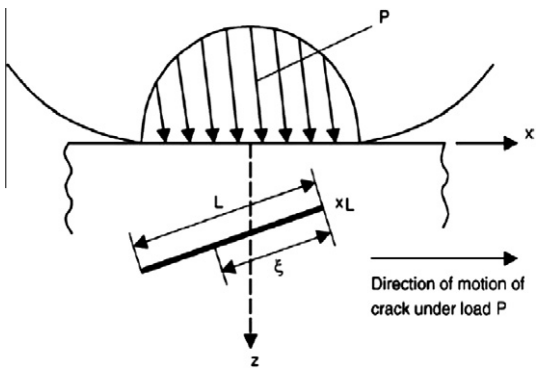

Fig. 1. Geometry of a crack moving under a stationary load ($L = 2a$, $x_L = x_{2a}$).

$$\tau_{eqv.} = \eta_{HV} \cdot \tau_{\max\_corr}$$
$$\eta_{HV} = \frac{\bar{\tau}_{\max}}{HV(z)}, \quad \tau_{\max\_corr} = \frac{\tau_{\max} \cdot \delta_K}{\psi}, \quad \psi = e^{-4.3\varepsilon}, \tag{3}$$
$$\delta_K = (K_t - 1) \cdot \eta + 1$$

where η_{HV} represents the hardness effect, $\tau_{\max\_corr}$ represents the corrected maximum shear stress, which includes the effects of porosity following Straffilini et al. [33]. $HV(z)$ represents the Vicker's hardness at depth z, $\tau_{\max}$ represents the maximum shear stress in the entire stress field, $\bar{\tau}_{\max}$ represents the equivalent maximum shear stress, ψ represents the reduction in load bearing section due to porosity, ε is the porosity fraction, K_t is the pore shape coefficient, and δ_K and η account for notch effects and the matrix microstructure.

The following expression can then be obtained:

$$\Delta K_{II} = U(a) \cdot \sqrt{\frac{2}{\pi \cdot 2a}} \int_0^{2a} \eta_{HV} \cdot \frac{\tau_{\max} \cdot ((K_t - 1) \cdot \eta + 1)}{e^{-4.3\varepsilon}} \cdot \left\{ \frac{2a - \xi}{\xi} \right\}^{1/2} d\xi \tag{4}$$

where $U(a)$ is a factor related to crack closure determined using the empirical formula of Newman [34]:

$$U(a) = 0.89 \cdot \left[1 + 0.11 \cdot \exp\left(\frac{a}{10} \right) \right] \tag{5}$$

In Eq. (4), $\tau_{\max}$ is calculated based on Mohr's circle theory, which is given as follows:

$$\tau_{\max} = \sqrt{\left[\frac{1}{2} (\sigma_x - \sigma_z) \right]^2 + \tau_{xz}^2}$$
$$\sigma_x(x,z) = \sigma_{x-n}(x,z) + \sigma_{x-t}(x,z) + \sigma_{x-r}(x,z) \tag{6}$$
$$\sigma_z(x,z) = \sigma_{z-n}(x,z) + \sigma_{z-t}(x,z) + \sigma_{z-r}(x,z)$$
$$\tau_{xz}(x,z) = \tau_{xz-n}(x,z) + \tau_{xz-t}(x,z)$$

where $\sigma_{x-n}(x,z)$, $\sigma_{z-n}(x,z)$ and $\tau_{xz-n}(x,z)$ are normal mechanical stresses, and $\sigma_{x-t}(x,z)$, $\sigma_{z-t}(x,z)$ and $\tau_{xz-t}(x,z)$ are tangential mechanical stresses. All the stresses are calculated using Smith and Liu's solution [35]. $\sigma_{x-r}(x,z)$ and $\sigma_{z-r}(x,z)$ are the residual stresses generated by surface treatments such as case hardening, which are computed using the empirical relationships between hardness and depth proposed by Lang [36], Tobe et al. [37] and Kato et al. [38]. In this study, the residual stresses are assumed to be [19]: (i) independent of the load cycle and (ii) equibiaxial, with equal normal components in the radial (perpendicular to the involute profile) and tangential (tangent to the involute profile) directions.

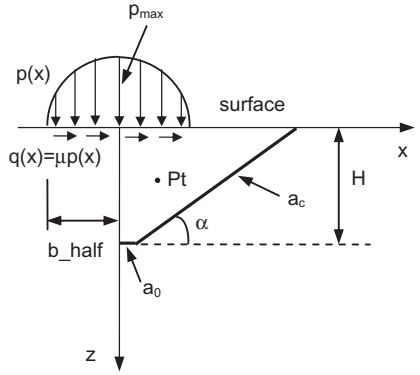

Fig. 2. Schematic of crack propagation.

Assuming $\tilde{x} = x/b\_half, \tilde{z} = z/b\_half$, the maximum shear stress $\tau_{\max,\,Pt}$ at a certain point $Pt(x,z)$ in the stress field can be calculated as follows (see Fig. 2.):

$$\tau_{\max,Pt}(\tilde{x},\tilde{z}) = \sqrt{\left[\frac{1}{2} (\sigma_x(\tilde{x},\tilde{z}) - \sigma_y(\tilde{x},\tilde{z})) \right]^2 + \tau_{xy}^2(\tilde{x},\tilde{z})} = \Delta p_{\max} \cdot F_{Pt}(\tilde{x},\tilde{z},\mu) \tag{7}$$

Therefore, the maximum shear stress $\tau_{\max}$ in the entire stress field can be obtained as follows:

$$\tau_{\max} = \Delta p_{\max} \cdot F_{Pt,\max}(\tilde{x},\tilde{z},\mu) \tag{8}$$

where $F_{Pt,\max}(\tilde{x},\tilde{z},\mu)$ is the maximum value of $F_{Pt}(\tilde{x},\tilde{z},\mu)$ in the stress field, which is a function of μ. The distribution of $F_{Pt,\max}(\tilde{x},\tilde{z},\mu)$ with μ is shown in Fig. 3:

The expression of the polynomial curve in Fig. 3 is given as:

$$F_{Pt,\max}(\mu) = 0.5318 \cdot \mu^2 - 0.0142 \cdot \mu + 0.3007 \tag{9}$$

Then

$$\tau_{\max} = \Delta p_{\max} \cdot (0.5318 \cdot \mu^2 - 0.0142 \cdot \mu + 0.3007)$$
$$\bar{\tau}_{\max} = \Delta \bar{p}_{\max} \cdot (0.5318 \cdot \mu^2 - 0.0142 \cdot \mu + 0.3007) \tag{10}$$

Using Eqs. 3, 4, and 10, the mode II stress intensity factor range at the crack tip can be calculated as follows:

$$\Delta K_{II} = U(a) \cdot \Delta p_{\max} \cdot \frac{\Delta \bar{p}_{\max} \cdot (0.5318 \cdot \mu^2 - 0.0142 \cdot \mu + 0.3007)^2 \cdot ((K_t - 1) \cdot \eta + 1)}{HV(a) \cdot e^{-4.3\varepsilon}} \cdot \sqrt{\pi a}$$
$$= U(a) \cdot \Delta p_{\max} \cdot G_{2a}(a, \mu, K_t, \eta, \varepsilon, HV_c, HV_s, z_{eff}, \Delta \bar{p}_{\max}) \tag{11}$$

where $G_{2a}(a, \mu, K_t, \eta, \varepsilon, HV_c, HV_s, z_{eff}, \Delta \bar{p}_{\max})$ is called the geometry function, HV_c represents the core hardness, HV_s represents the surface hardness, z_{eff} represents the effective case depth, μ is the coefficient of friction of the contact surfaces, $\Delta p_{\max}$ is the maximum contact pressure range, which is calculated from time domain simulations, and $\Delta \bar{p}_{\max}$ is the equivalent maximum contact pressure range (Equ. Max. Cont. Pres. Ran.), which is given in Eq. (15).

In Eq. (11), the random nature of the maximum contact pressure range $\Delta p_{\max}$ leads to a random cyclic stress intensity factor range ΔK_{II} because of their linear relationship. This fundamental variability of ΔK_{II} may however be taken into account by using the average crack growth rate obtained by weighting the crack growth rates for given ΔK_{II} values with their probability of occurrence.

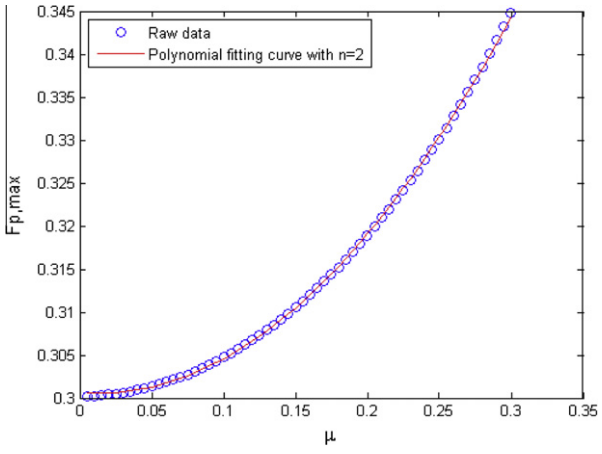

Fig. 3. The distribution of $F_{Pt,\max}(\tilde{x},\tilde{z},\mu)$.

Table 1
Basic data for spur gear geometry.

Number of teeth		Face width (mm)		Module (mm)	Coefficient of profile shift		Pressure angle	Torque (N m)
Z_1	Z_2	b_1	b_2	4.5	x_1	x_2	20°	183.4
16	24	14	14		0.182	0.171		

Table 2
Chemical composition of 42CrMo4.

C (%)	0.43
Si (%)	0.22
Mn (%)	0.59
Cr (%)	1.04
Mo (%)	0.17

Table 3
Material parameters.

42CrMo4					
E (Mpa)	206,000	τ'_f (MPa)	1051	HV_s (Mpa)	595
v	0.3	b	−0.08	y_{eff} (mm)	1.0
G (Mpa)	80,000	σ_y (Mpa)	900		
σ'_f (Mpa)	1752	HV_c (Mpa)	300		

Table 4
Parameters for calculating τ_{max_corr}.

k_t	3
η	0.7
ε	0.11

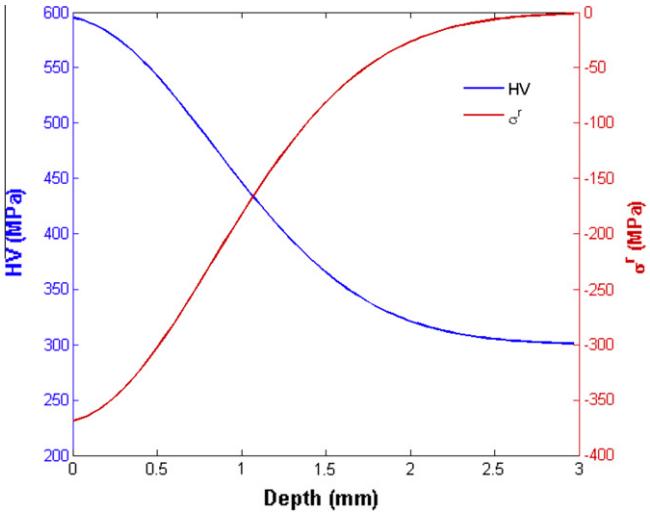

Fig. 4. Micro-hardness distribution (HV) and residual stress (σ^r) profiles for different case depth.

Using Eqs. (1) and (11), the following expression can be obtained:

$$\frac{da}{dN} = \int_0^{\infty} \frac{da}{dN}(\Delta k_{II}) \cdot f_{\Delta k_{II}}(\Delta k_{II}) \cdot d(\Delta k_{II}) = C \cdot G_{2a}^{m}(a, \mu, K_t, \eta, \varepsilon, HV_c, HV_s, z_{eff}, \Delta\bar{p}_{\max}) \cdot U^{m}(a) \cdot \int_0^{\infty} \Delta p_{\max}^{m} \cdot f_{\Delta p_{\max}}(\Delta p_{\max}) d\Delta p_{\max} \quad (12)$$

Table 5
Comparison between the experimental and numerical results.

Numerical model (current)	Numerical model (Glodez et al. [16])	Experiment (Glodez et al. [16])	
N_P (cycle)	N_P (cycle)	Probability $P(N)$ in (%)	N (cycles)
3.519×10^6	3.451×10^6	50	$2.900–3.494 \times 10^6$
		70	$2.771–3.622 \times 10^6$
		90	$2.629–3.765 \times 10^6$
		95	$2.590–3.803 \times 10^6$
		99	$2.558–3.835 \times 10^6$

Table 6
General description of the wind turbine.

Type	Three blade up wind
Power rating	750 kW
Rotor diameter	48.2 m
Rated rotor speed	22/15 rpm
Power regulation	Stall
Tower	Welded tubular steel
Nominal hub height	55 m
Cut-in wind speed	3 m/s
Rated wind speed	16 m/s
Cut-out wind speed	25 m/s
Design wind class	IEC Class II
Design life	20 years

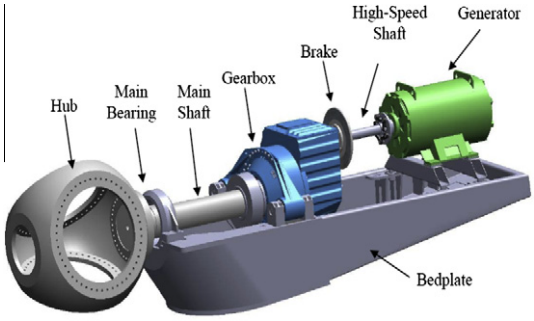

Fig. 5. Drivetrain configuration of the wind turbine.

Then:

$$\int_{a_0}^{a_c} \frac{1}{G_{2a}^{m}(a, \mu, K_t, \eta, \varepsilon, HV_c, HV_s, z_{eff}, \Delta\bar{p}_{\max}) \cdot U^{m}(a)} da = C \cdot N_p \cdot \int_0^{\infty} \Delta p_{\max}^{m} \cdot f_{\Delta p_{\max}}(\Delta p_{\max}) d\Delta p_{\max} \quad (13)$$

Assuming:

$$P_{lng} = \int_0^{\infty} \Delta p_{\max}^{m} \cdot f_{\Delta p_{\max}}(\Delta p_{\max}) d\Delta p_{\max} \quad (14)$$

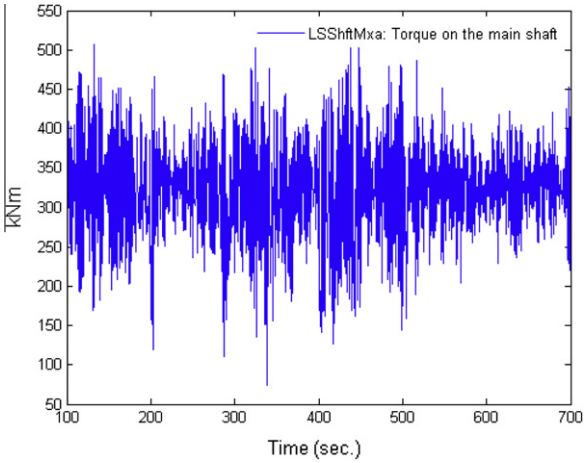

Fig. 6. Time series of torque on the main shaft (U_w = 16 m/s).

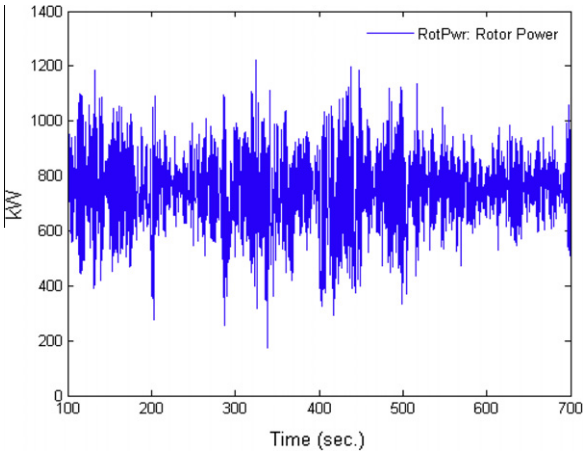

Fig. 7. Time series of rotor power (U_w = 16 m/s).

the equivalent maximum contact pressure range is defined as follows:

$$\Delta\bar{p}_{\max} = \left(\int_0^{\infty} \Delta p_{\max}^m \cdot f_{\Delta p_{\max}}(\Delta p_{\max}) d\Delta p_{\max} \right)^{1/m} \quad (15)$$

Table 7
Model information of gears.

Item	Sun gear	Planetary gear	Ring gear
Normal module	10	10	10
Number of tooth	21	39	39
Attack angle (°)	20	20	20
Helix angle (°)	7.5	7.5	7.5
Base diameter (mm)	199	369	937
Pitch diameter (mm)	216	400	1016
Face width (mm)	220	220	220

Finally, the following expression can be obtained and used to predict the number of cycles for crack propagation:

$$N_p = \int_{a_0}^{a_c} \frac{1}{C \cdot G_{2a}^m(a, \mu, K_t, \eta, \varepsilon, HV_c, HV_s, z_{eff}, \Delta\bar{p}_{\max}) \cdot U^m(a) \cdot \Delta\bar{p}_{\max}^m} da \quad (16)$$

In Eq. (16), the effects of random environmental loads are considered through $\Delta\bar{p}_{\max}$. An additional benefit of this model is that it can be used to obtain the so-called 'limit state function' to perform reliability-based contact fatigue design of gears (see Eq. (13)), which has been commonly used in the aerospace, nuclear, and offshore oil and gas industries during past decades. More details about reliability theory can be found in [39].

2.3. Validation of the deterministic models

The proposed model was applied to the spur gear example defined in Table 1. The gear is composed of high strength steel alloy (42CrMo4) with an average prior austenite grain diameter $D \cong 50$ μm and a surface hardness of approximately 55 HRc. Its chemical composition (wt.%) is given in Table 2. The relevant material parameters are given in Table 3 and Table 4. Additional details can be found in [19].

The test of the pinion-gear pair was performed by Glodez et al. [16] using a FZG back to back test rig, with a pinion torque of 183.4 Nm and a pinion speed of 2175 rpm. The dip lubricant was applied to the gears, and the temperature of the lubricant was controlled. The lubricant was INA-EPOL SP 220 with kinematic viscosities of ν_{40} = 220 mm^2 s^{-1} and ν_{100} = 17.9 mm^2 s^{-1} at 40 and 100 °C, respectively. The gears were periodically inspected to detect the occurrence of pitting on the tooth flanks. The test was stopped

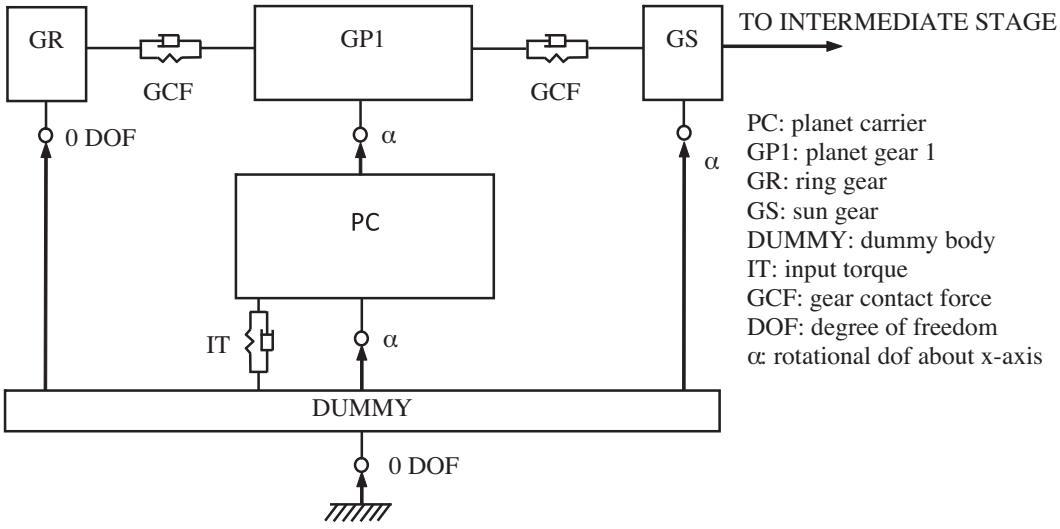

Fig. 8. Topology diagram of gearbox model in SIMPACK.

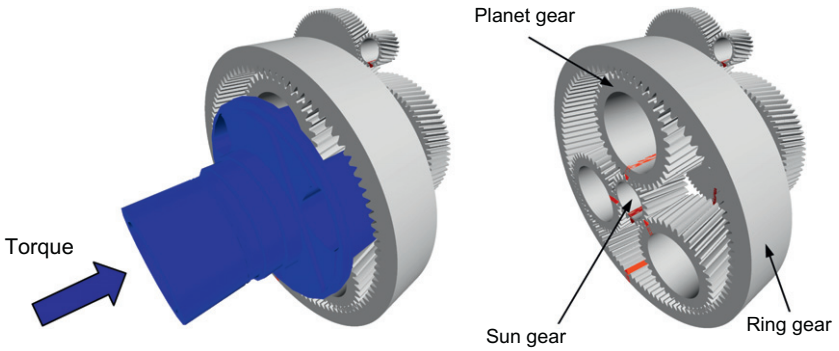

Fig. 9. Gearbox model in SIMPACK.

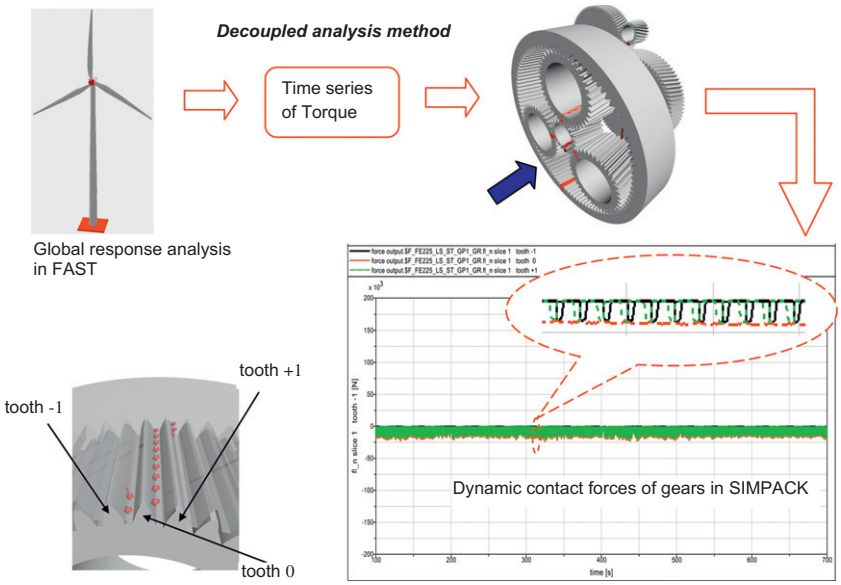

Fig. 10. Scheme of procedure for gear dynamic contact force.

and the corresponding number of loading cycles was recorded whenever pits larger than 0.5 mm were observed. The material constants were $C = 4.90924 \times 10\ \text{mm}/(\text{cycle}\,(\text{MPa})\,\text{mm}^{0.5})^m$ and $m = 3.05$. The value of C was estimated using the relationship between the crack tip plastic displacement δ_{pl} and the stress intensity factor K. The value of m was adjusted from 3.0 to 3.05. Additional details can be found in [16]. The coefficient of friction μ was approximately 0.04, which can also be estimated using empirical formulas [40,41]. The nominal maximum contact pressure is taken as 1406 MPa [16] according to the DIN standard procedure [4]. It is noted that P_{lng} and $\Delta\bar{p}_{\max}$ are simplified as $P_{lng} = \Delta\bar{p}_{\max} = p_{\max} = 1406$ MPa for the test conditions.

Using Smith and Liu's solution [35] and Eq. (6), the maximum shear stress $\tau_{\max}$ is calculated to be 423.212 MPa. The crack propagation angle α is taken as 17.2° based on Leng et al. [42] and Agha [26]. The initial crack is assumed to be parallel to the surface and its half length is taken as $a_0 = 12.5\ \mu\text{m}$ [16] at a depth $H = 0.1432$ mm under the contact surface, where the cracks are assumed to initiate at the point where the ratio of the maximum shear stress to hardness is greatest [19,29,32,42,43]. Fig. 2 shows a schematic of the crack propagation. Fig. 4 shows the relationship between the micro-hardness distribution and the residual stress profiles. Table 5 compares the results of the numerical models with the experiments; the results verify the validity of the predictive

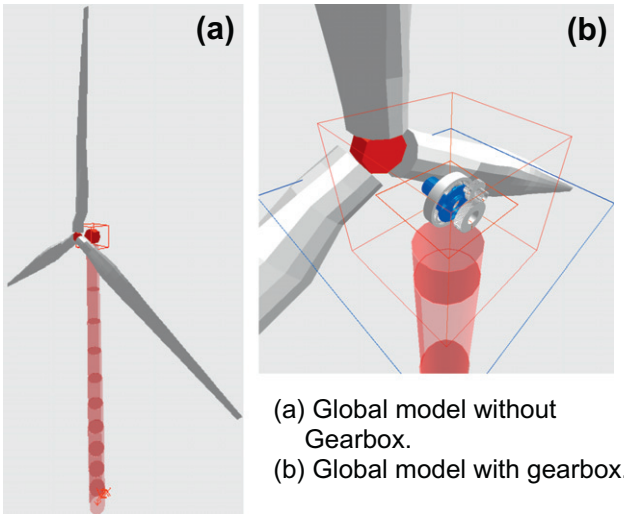

Fig. 11. Scheme of two different wind turbine models in SIMPACK.

models described above. $P(N)$ represents the probability that pitting will occur on the teeth flanks in the load cycle interval $[N_1, N_2]$.

Table 8
Comparison of the mean values and the standard deviations of the torques in the main shaft.

Wind speed (mean)	Torque with gearbox (N m)		Torque without gearbox (N m)	
	Mean	Std.	Mean	Std.
8 m/s	1.17e+05	7.05e+04	1.17e+05	7.61e+04
16 m/s	3.20e+05	4.12e+04	3.20e+05	5.78e+04
20 m/s	3.23e+05	3.44e+04	3.23e+05	4.81e+04

Table 9
Comparison of the mean values and the standard deviations of the total circumferential forces generated in meshing gears.

Wind speed (mean)	Total circumferential force with global model (N)		Total circumferential force without global model (N)	
	Mean	Std.	Mean	Std.
8 m/s	6.74e+05	3.69e+04	6.74e+05	4.01e+04
16 m/s	1.73e+05	2.26e+04	1.73e+05	3.20e+04
20 m/s	1.75e+05	1.87e+04	1.75e+05	2.67e+04

3. Gear contact fatigue analysis based on time domain simulations

This study used, a 750 kW land-based wind turbine from the Gearbox Reliability Collaborative (GRC) project, which is coordinated by the National Renewable Energy Laboratory (NREL) in Colorado, USA, as the case study. A general description of the wind turbine is given in Table 6, and additional details can be found in [44]. The configuration of the drive-train system of the wind turbine is shown in Fig. 5, and additional details can be found in [45].

3.1. Global response analysis of a land-based NREL 750 kW wind turbine

In this study, global aero-elastic simulations of the wind turbine were performed using the FAST code from NREL [20]. FAST is an aero-elastic code that computes the coupled structural response of a wind turbine under aerodynamic load effects. In the FAST simulations, the wind turbine is assumed to be rigidly fixed to the ground. The mechanical components in the drive-train system are modeled as springs and dampers. The turbulent wind fields are generated using the Kaimal [46] spectrum and exponential coherence model, and the turbulent intensity is taken as class A [47]. The range of 1-h mean wind speed U_w is 4–24 m/s with an increment of 2 m/s. To minimize the statistical uncertainties due to the time domain simulation, 20 simulations are performed using different random seed numbers for each wind speed. Each wind speed is simulated for 700 s, and the first 100 s is discarded. Additional details can be found in [48]. Fig. 6 shows an example of a time series of torque on the main shaft in the FAST simulation, and Fig. 7 shows the relevant time series of rotor power.

3.2. Contact force analysis of the sun gear and the planet gears

In this study the time series of the main shaft torques obtained from FAST simulation are used as inputs to a multibody gearbox model in SIMPACK [21]. SIMPACK is a multi-purpose multibody code with special features available to model gearboxes. Each component of the gearbox is modeled as a rigid body and is interconnected using joints and force elements. The topology diagram of the gearbox model is shown in Fig. 8. Table 7 presents the basic model information of the gears. Fig. 9 shows the gearbox model in SIMPACK, and Fig. 10 shows the procedure used in the analysis. The gear pair force element in SIMPACK, FE225, is used to model the gear contacts. FE225 models gear contacts as a series of discrete springs and dampers. The gear stiffness is calculated in accordance with ISO 6336-1 [49]. The contact forces in meshing gears are obtained using the slicing method. An application of this method can be found in [50], and additional details about the dynamic contact force analysis of the gears can be found in [48].

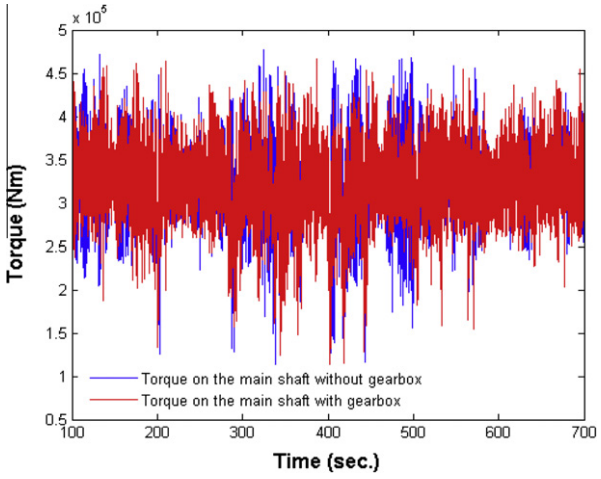

Fig. 12. Comparison of results of the torques in the main shaft (U_w = 16 m/s).

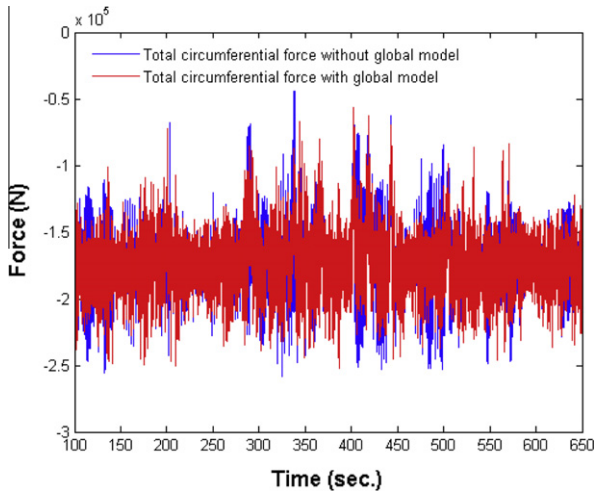

Fig. 13. Comparison of results of the total circumferential forces generated in the meshing gears.

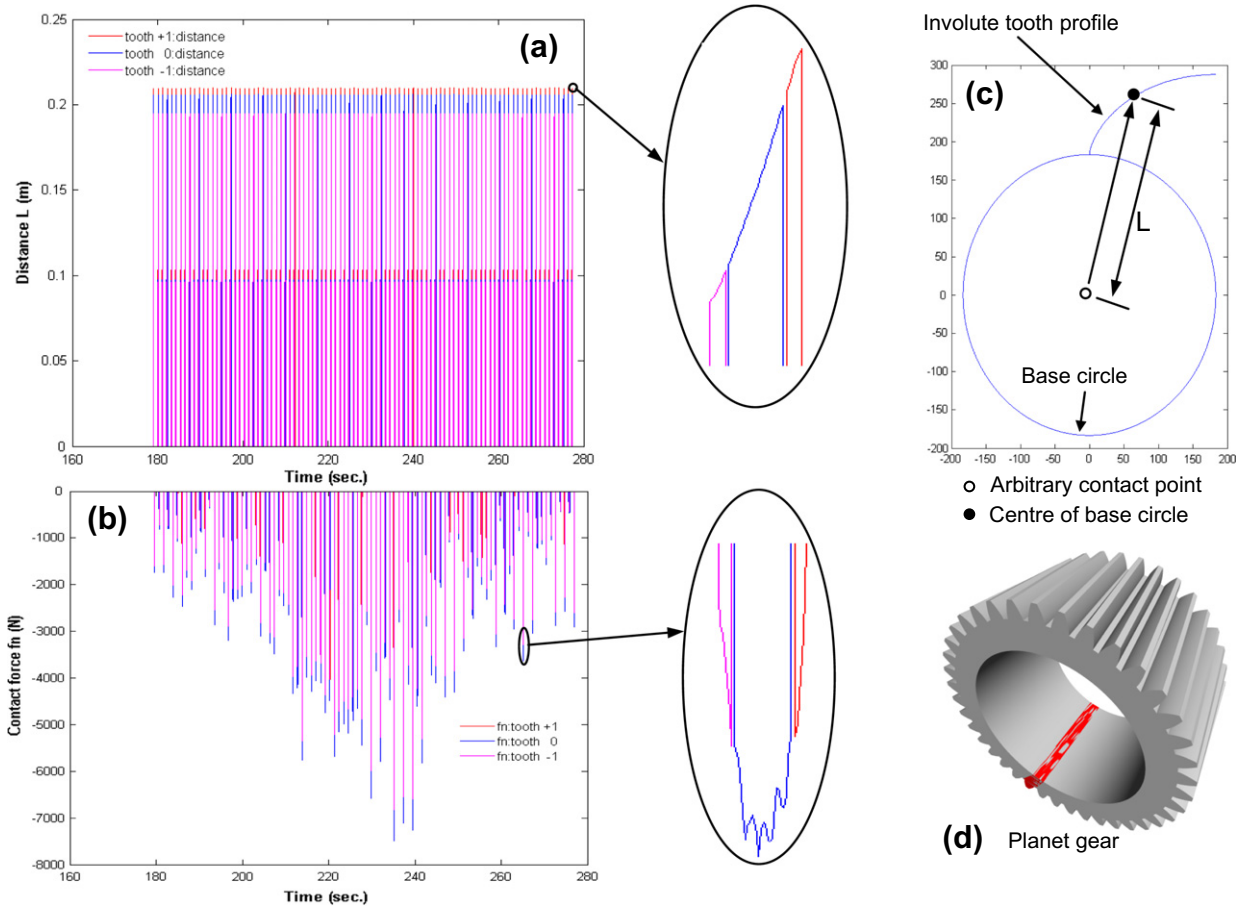

Fig. 14. Schematic of post-processing of the time domain simulation results in SIMPACK. (a) Route of contact point. (b) Contact force distribution with the route of contact point (fn: contact force). (c) Schematic of *L*. (d) Planet gear model in SIMPACK.

3.2.1. Comparison between coupled and decoupled analysis methods

As shown in Fig. 10, the decoupled analysis method is used to calculate the dynamic contact forces of the gears because time domain simulations are time consuming. A fully coupled wind turbine model was also made in SIMPACK (Fig. 11b), and the simulation results of the decoupled method and the fully coupled model were compared. The main purpose was to check (i) the effects of the gearbox on the torque calculations and (ii) the effects of the global model on the gear contact force calculations. Table 8 compares the results of the mean values and the standard deviations of the torques in the main shaft for three different wind speeds, and Table 9 shows the mean values and the standard deviations of the total circumferential forces generated in meshing gears for three different wind speeds. Fig. 12 shows an example of the time series of the torques in the main shaft for the two methods, and Fig. 13 shows an example of the time series of the total circumferential forces generated in meshing gears for the two methods. These comparisons show that the mean values for the decoupled and fully coupled analysis methods are nearly identical. However, the standard deviations for the decoupled method are greater than those for the fully coupled method.

3.2.2. Post-processing of SIMPACK results

In the gearbox model considered in this study, the sun gear has 21 teeth, and each planet gear has 39 teeth. To perform the time-domain based gear contact fatigue analysis, the time series of the contact forces for each gear tooth should be obtained by postprocessing the MBS simulation results. In SIMPACK, an arbitrary gear tooth experiences three different stages in one meshing. These

Table 10
Four different GG models.

Item	a_w	b_w	c_w (m/s)	U_m (m/s)
Case 1	2.143	1.4	1.52	2.5
Case 2	2.143	1.4	1.83	3.0
Case 3	2.143	1.4	2.13	3.5
Case 4	2.143	1.4	2.45	4.0

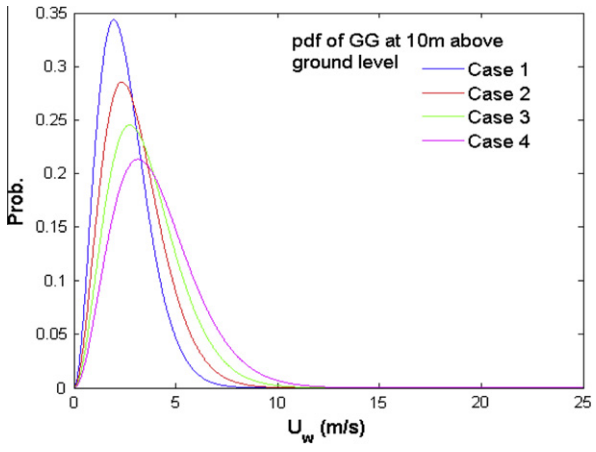

Fig. 15. Pdf of the GG model for four different environmental cases.

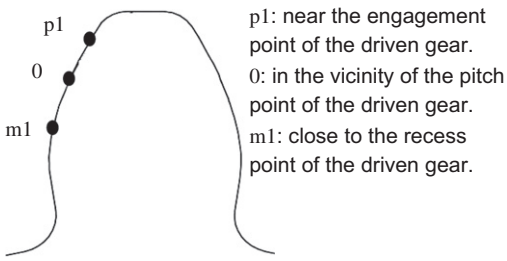

Fig. 16. Positions of the considered points on the profile (driven gear-sun gear).

stages are the engagement, middle and recess stages, which are denoted 'tooth−1', 'tooth 0', 'tooth + 1' (as shown in Fig. 10). Fig. 14 shows the postprocessing results of a gear tooth for different cycles at U_w = 4 m/s. The cases of other wind speeds are similar but are not shown here. For each wind speed, a critical gear tooth is identified in terms of the maximum mean contact force. A dummy gear tooth is defined, and the time series of the contact forces of the critical gear tooth for each wind speed are all applied to this dummy gear tooth, which is taken to be representative of all the teeth of the sun gear or the planet gear. Thus the long-term contact fatigue results should be conservative. In addition, a simpler method of performing the time domain-based long-term contact fatigue analysis of gears was suggested by Dong et al.; more details can be found in [48].

In this study only the torques in the main shaft are considered. Xing et al. [51], suggested that the contribution from non-torque loading (e.g. bending moment and shear forces) to the gear contact force calculation might be in the range of 10–20%; this will be investigated in future work. In addition, a simple rigid body gearbox model is used in this paper, more refined gearbox models, e.g. with flexible components modeled, might be applied in future work. For the actual tooth load distribution, the bearing compliance and clearances are important. Furthermore, the compliance of the main shaft, low speed shafts are also important in the tooth contact loads in the low-speed planetary stage. More details about various model fidelity studies for various applications could be found in [52–55]. The detailed tooth load distribution analysis due to various model fidelity and its effects on gear contact fatigue analysis of a wind turbine drivetrain would be performed in future work.

3.3. Long-term probability distribution analysis of contact pressure range

In general, the probability distribution of the mean wind speeds can be described by the Rayleigh distribution, the Weibull distribution, and the generalized gamma distribution. Recently Kiss and

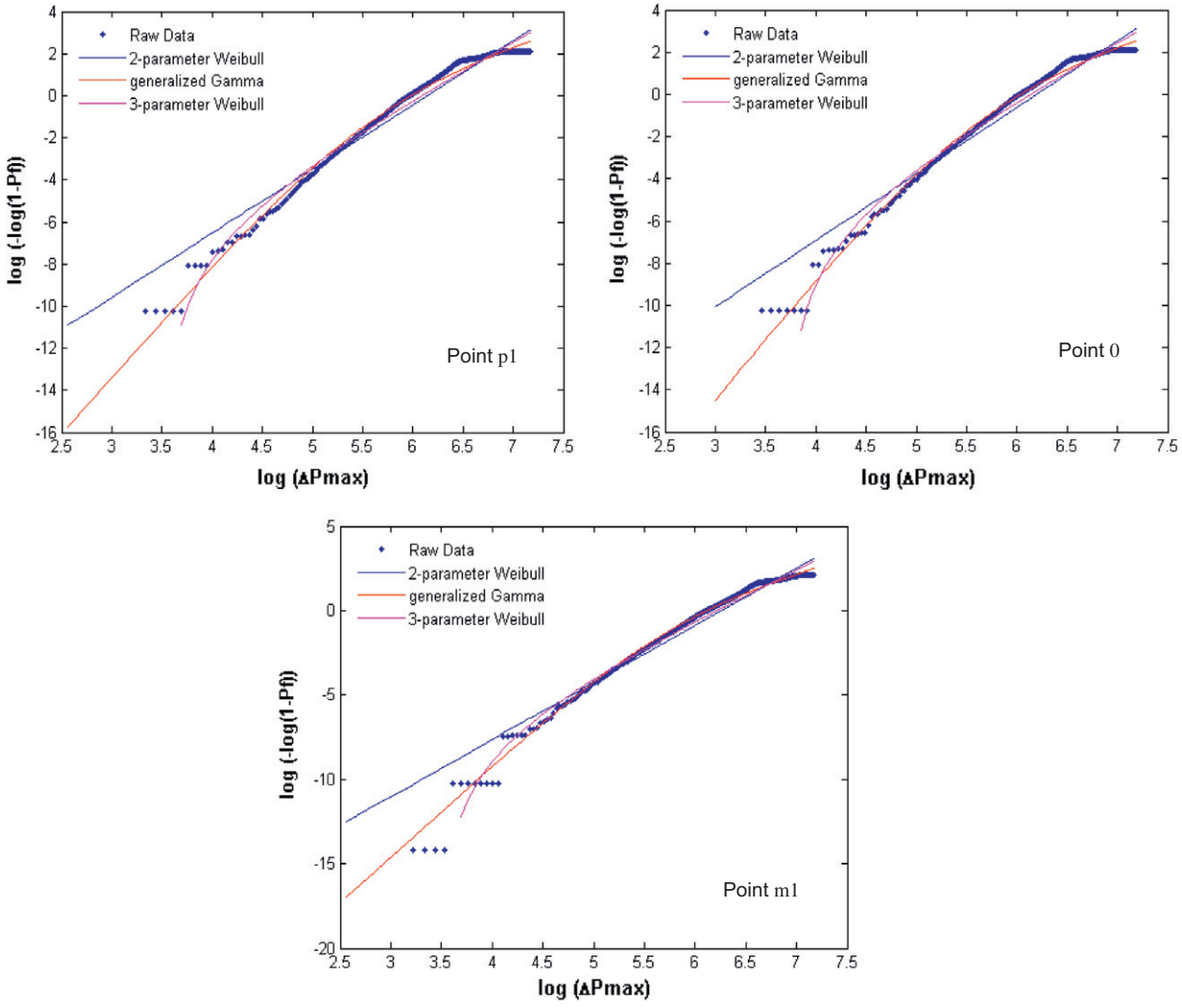

Fig. 17. Long-term results of the maximum contact pressure range Δp_{max} generated in the representative sun gear tooth for case 1.

Janosi [56] performed a comprehensive study on the wind speed probability distribution over the sea and land in Europe based on the ERA-40 database, which covers a time period of 44 years between 1 September 1958 and 31 August 2002 [57]. Based on their work, the Weibull model performs well over the seas but fits the data poorly over major inland areas in Europe. However, the generalized gamma (GG) model fits the data well nearly everywhere; the fit is especially good for the high speed tail of the distribution, which is essential in wind power estimations. Therefore, the GG model is used to describe the probability distribution of the mean wind speed in this study, which is given as follows:

$$f_{GG}(U) = \frac{b_w}{c_w \Gamma(a_w)} \left(\frac{U_w}{c_w}\right)^{a_w b_w - 1} \exp\left(-\left(\frac{U_w}{c_w}\right)^{b_w}\right) \tag{17}$$

where a_w, b_w, c_w are the parameters used in the GG model, and U_w is the wind speed at 10 m above ground level. The wind speed at the hub height U_{hub} is calculated using the following equation [47]:

$$U_{hub} = U_w \cdot \left(\frac{z_w}{z_{hub}}\right)^{\alpha} \tag{18}$$

where $z_w = 10$, and z_{hub} is the hub height. For land-based wind turbines, $\alpha = 0.2$.

Hoogwijk et al. [58] assessed the regional and global geographical, technical and economic potential of onshore wind energy using a grid cell approach based on the available Climate Research Unit (CRU) database [59,60] in which approximately 80% of the global surface area has an annual average wind speed of less than 4 m/s at a height of 10 m (e.g., sub-Saharan Africa and the entire Indian continent). In this study four different mean wind speed cases are considered (Table 10). The values of the parameters are obtained from [57]. U_m represents the mean wind speed at 10 m. Fig. 15 shows the probability density distributions of the four GG models.

This study mainly considered the normal operating condition of the NREL 750 kW land based wind turbine, which is defined as design load case 1.2 (DLC 1.2) in IEC-61400-1[47]. Eleven different wind speeds (4–24 m/s) were considered, and 20 simulations were performed for each wind speed. Three different probability functions were used to fit the long-term statistical distribution of the maximum contact pressure range $\Delta p_{\max}$, including the two-parameter Weibull distribution, the generalized gamma distribution and the three-parameter Weibull distribution. Fig. 17 shows the long-term results of $\Delta p_{\max}$ at three different contact locations on the representative sun gear tooth for case 1. The results of cases 2–4 are similar to case 1 and are not shown here. The probability func-

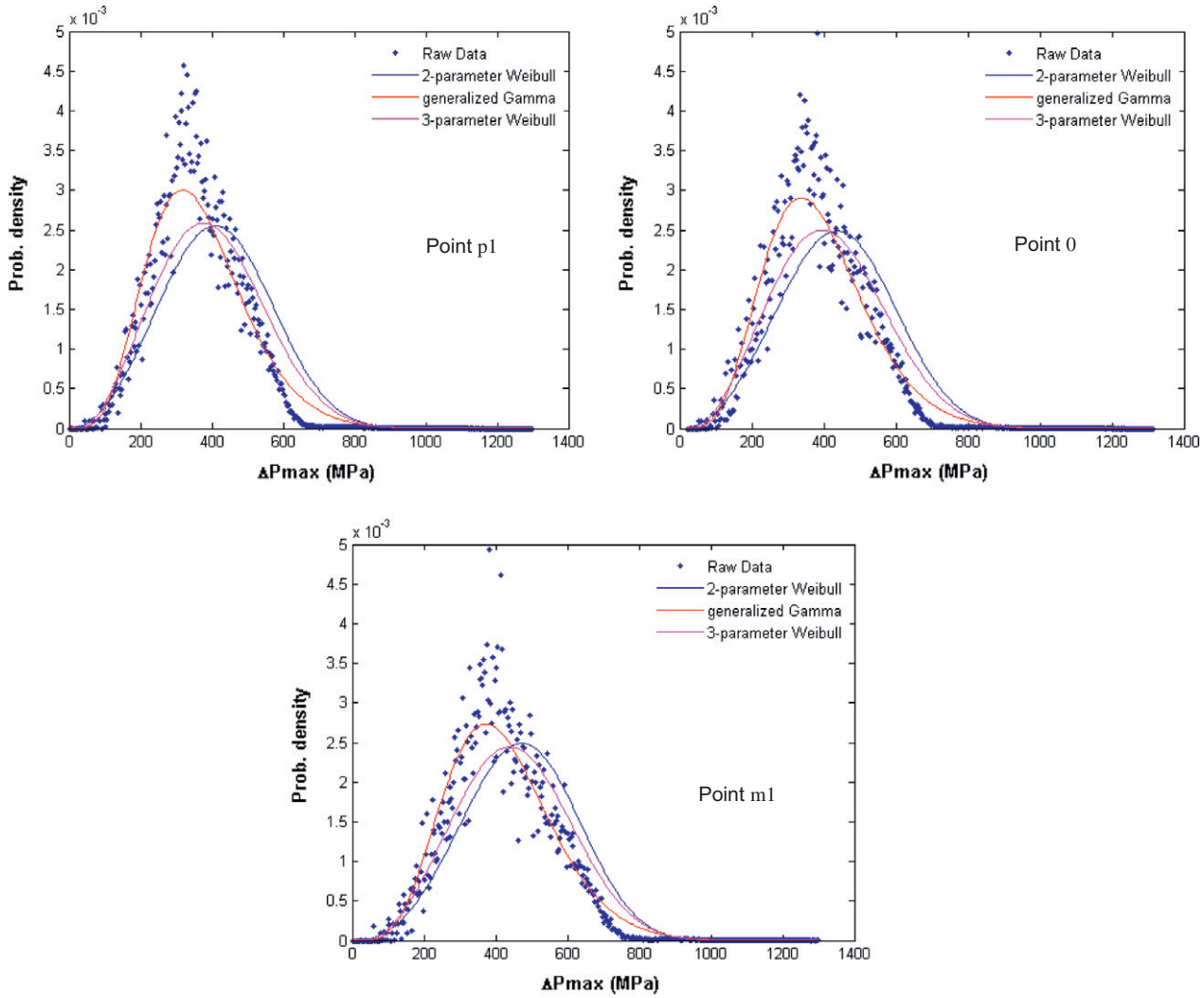

Fig. 18. Probability density distribution of the maximum contact pressure range $\Delta p_{\max}$ generated in the representative sun gear tooth for case 1.

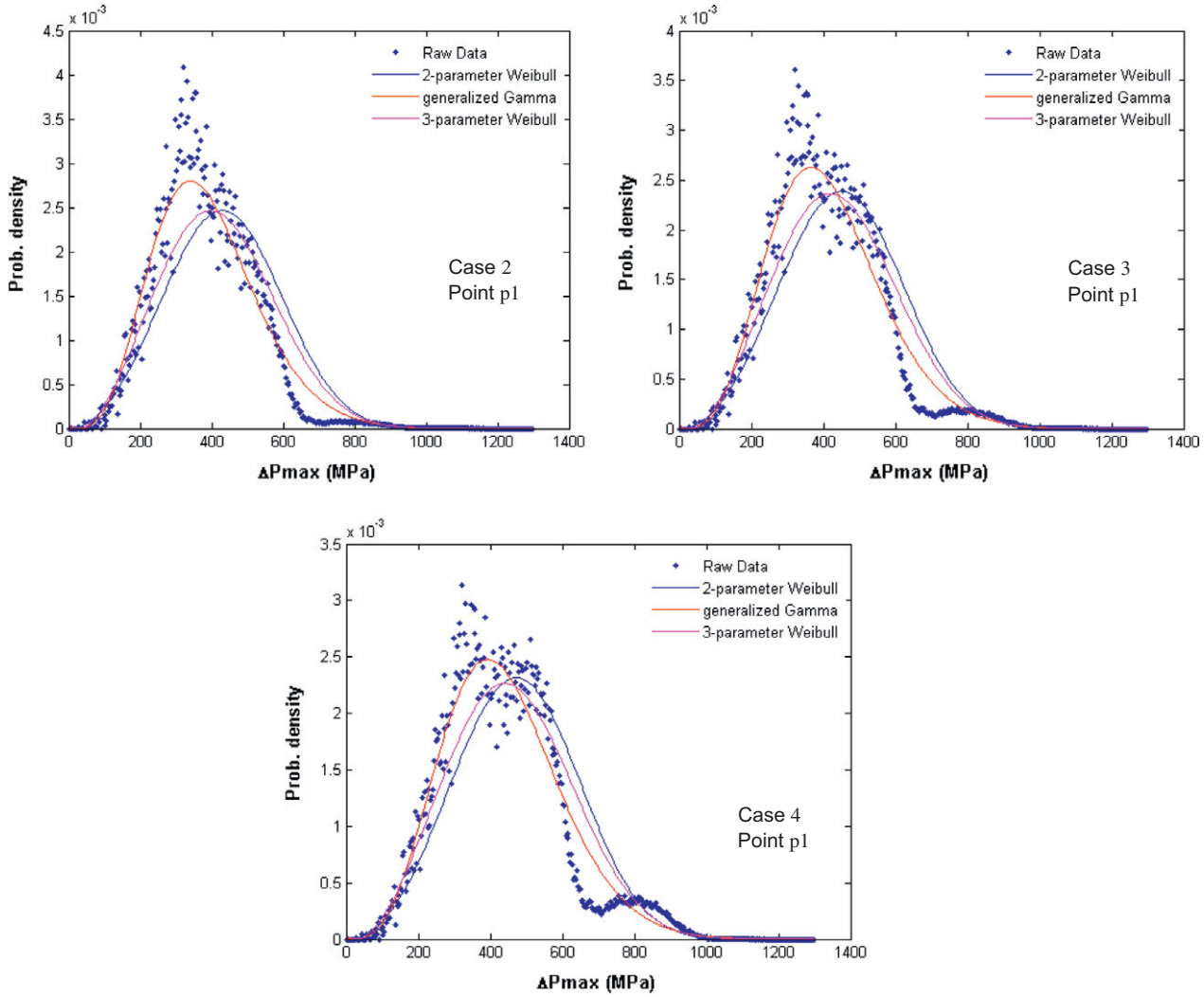

Fig. 19. Probability density distribution of the maximum contact pressure range $\Delta p_{\max}$ generated in the representative sun gear tooth for cases 2–4.

tions fit the data well, but the two-parameter Weibull distribution is much simpler than the generalized gamma and the three-parameter Weibull distributions. Fig. 18 shows the relative probability density distributions of $\Delta p_{\max}$, and Fig. 19 shows the probability density distributions of $\Delta p_{\max}$ at contact point p1 on the representative sun gear tooth for cases 2–4. There is a small wave crest from 800 MPa to 1000 MPa that is more significant with increasing U_m. The main reason for this is shown in Fig. 20. As stall-regulated control is applied, the maximum contact pressure range $\Delta p_{\max}$ is mainly located between 800 MPa and 1000 MPa for high wind speeds (12–24 m/s). In addition, the raw data in Figs. 17–19 appears to be too condensed. One of the main reasons for this is due to the assumption that the winds are always from the same direction, which is also the simplification of the design load case DLC 1.2 in IEC-61400-1[47]. In practice, the raw data should be more scattered. The results for the planet gears are similar to those of the sun gear, and are not shown here.

4. Results

The contact fatigue lives of the sun gear and the planet gear are estimated at three different contact points (as shown in Fig. 16) based on the life prediction models and analysis procedures described above. It is assumed that the sun gear and the planet gear are both made of 42CrMo4. The characteristic properties of this material are given in Tables 2–4. The fit parameters of the two-parameter Weibull distribution at the different contact points for four different environmental cases are given in Table 11. A is the scale parameter of the Weibull distribution, and B is the dimensionless shape parameter, which changes slightly with the different environmental cases. The equivalent maximum contact pressure $\Delta \bar{p}_{\max}$, which is used to predict the crack propagation period, is given in Table 12. In practice, $\Delta \bar{p}_{\max}$ should be multiplied by a safety factor, which is not used in this study. The practical cycle numbers for the four environmental cases obtained from the time domain simulations are given in Table 13. These results show that the cycle numbers increase with increasing U_m (from case 1 to case 4), which is mainly due to the increased probabilities of wind speeds greater than the cut-in wind speed (from case 1 to case 4). This is because the wind turbine considered in this study is a fixed-speed wind turbine. The rated rotor speed for different wind speeds is nearly constant. The estimated cycle numbers using Eq. (16) for the four environmental cases are given in Table 14 and decrease with increasing U_m (from case 1 to case 4); this is because $\Delta \bar{p}_{\max}$ increases, as shown in Table 12. Tables 13 and 14 show that the planet gear is safe for the four environmental cases. The sun gear is safe for case 1, but may fail in cases 2–4. The environmental loads have a large effect on the contact fatigue lives of the gears. In

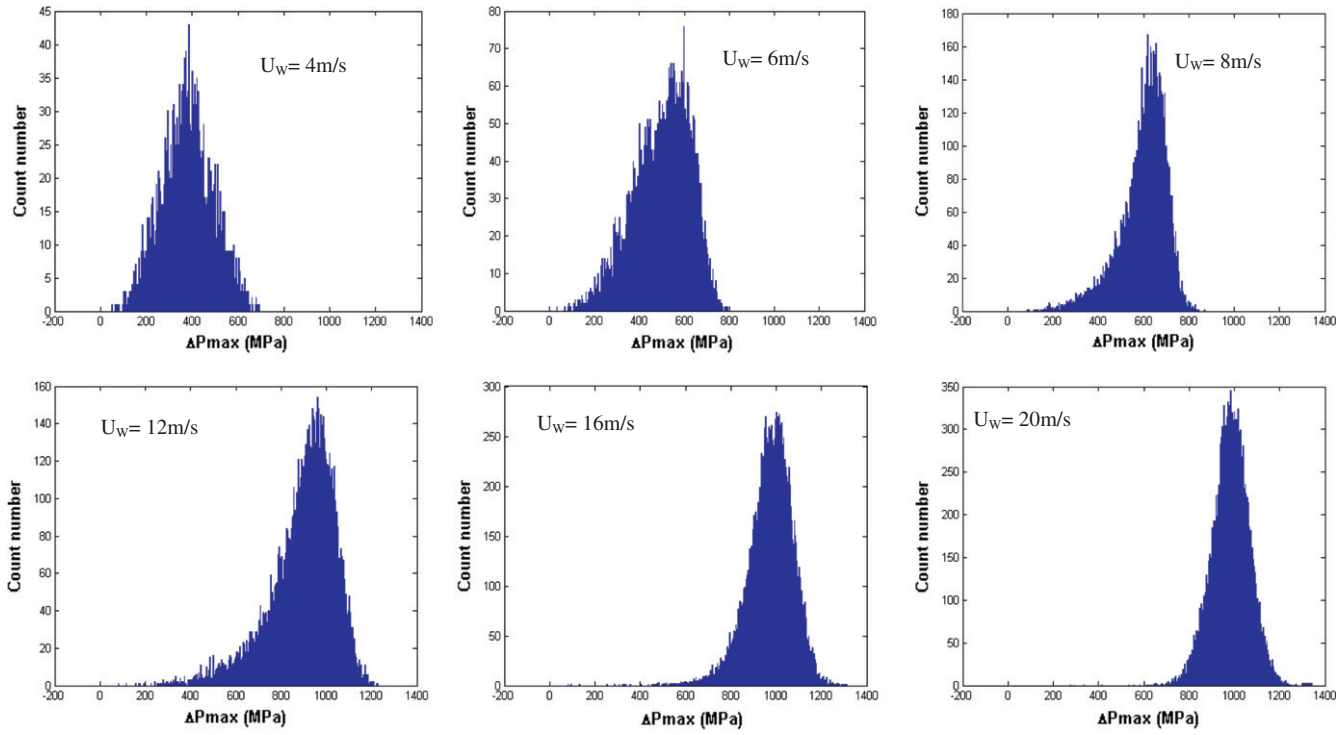

Fig. 20. Histograms of the maximum contact pressure range Δp_{max} of the representative sun gear tooth for different wind speeds.

addition, the recess area (near contact point m1) of the sun gear appears to be the critical location compared with the pitch point and the engagement areas. This is because the equivalent radius R at point m1 is much smaller than at points 0 and p1; it is only 74.55% of the value of R at point p1. In addition, material properties and fabrication techniques have large effects on the contact fatigue lives of gears. Table 15 shows the estimated pitting service lives of the sun gear for case 3 for different values of R based on the assumption that the contact forces generated in the meshing gears do not change. The estimated contact fatigue life for or contact points p1, 0 and m1 increase by a scale of 34.86%, 35.94% and 37.08%, respectively, if R increases by 15%.

Finally, it should be noted that the geometry of the gearbox model is obtained from NREL's 750 kW land-based Gearbox Reliability Collaborative wind turbine, while the sun gear and the planet gears are assumed to be composed of 42CrMo4, and the relative properties are taken from [16,19]. Therefore the gearbox model used in this case study is not a real design model. The main purpose of the work was to investigate the effects of environmental conditions on gear contact fatigue lives in the drive-train of a wind turbine. In addition, the mean wind speeds (U_m) of the four environmental cases are much smaller than the rated wind speed (16 m/s) of the wind turbine. Therefore, the contributions from high wind speeds (i.e. U_{hub} > 15 m/s) to gear contact fatigue dam-

Table 11
Fitting parameters of the two-parameter Weibull distribution.

Item	Position	Case 1		Case 2		Case 3		Case 4	
		A (MPa)	B	A (MPa)	B	A (MPa)	B	A (MPa)	B
Sun gear	p1	466.83	3.05	488.21	3.08	509.47	3.12	531.69	3.16
	0	492.38	3.15	515.09	3.17	537.87	3.20	561.84	3.23
	m1	524.64	3.38	548.93	3.36	573.98	3.36	600.92	3.36
Planet gear	p1	529.88	3.22	559.71	3.07	581.88	3.11	608.05	3.15
	0	477.53	2.85	504.11	2.72	531.95	2.71	561.65	2.75
	m1	456.13	2.95	477.84	2.91	507.76	2.81	535.63	2.82

Table 12
Equivalent maximum contact pressure $\Delta\bar{p}_{max}$.

Item	Position	R (m)	$\Delta\bar{p}_{max}$ (MPa)			
			Case 1	Case 2	Case 3	Case 4
Sun gear	p1	0.0279	466.91	487.57	507.95	529.10
	0	0.0271	490.36	512.53	534.58	557.61
	m1	0.0208	518.10	542.43	567.29	593.82
Planet gear	p1	0.0208	526.13	559.14	580.39	605.53
	0	0.0271	482.43	513.34	542.31	571.00
	m1	0.0279	458.32	481.17	514.29	542.04

Table 13
Practical cycle numbers based on time domain simulation.

Item	Position	Cycle numbers							
		Case 1		Case 2		Case 3		Case 4	
		Per second	20 years	Per second	20 years	Per second	20 years	Per second	20 years
Sun gear	p1	0.598 (×3)	1.13e+9	0.853 (×3)	1.61e+9	1.05 (×3)	1.99e+9	1.22 (×3)	2.31e+9
	0	0.598 (×3)	1.13e+9	0.853 (×3)	1.61e+9	1.05 (×3)	1.99e+9	1.22 (×3)	2.31e+9
	m1	0.598 (×3)	1.13e+9	0.853 (×3)	1.61e+9	1.05 (×3)	1.99e+9	1.22 (×3)	2.31e+9
Planet gear	p1	0.321	2.03e+7	0.459	2.90e+8	0.569	3.59e+8	0.662	4.18e+8
	0	0.321	2.03e+7	0.459	2.90e+8	0.569	3.59e+8	0.662	4.18e+8
	m1	0.321	2.03e+7	0.459	2.90e+8	0.569	3.59e+8	0.662	4.18e+8

Table 14
Estimated pitting service life of the sun gear and the planet gears.

Item	Position	N_p			
		Case 1	Case 2	Case 3	Case 4
Sun gear	p1	2.92e+9	2.25e+9	1.75e+9	1.36e+9
	0	2.17e+9	1.66e+9	1.28e+9	9.88e+8
	m1	1.54e+9	1.17e+9	8.90e+8	6.74e+8
Planet gear	p1	1.41e+9	9.72e+8	7.75e+8	5.99e+8
	0	2.39e+9	1.64e+9	1.17e+9	8.54e+8
	m1	3.27e+9	2.43e+9	1.62e+9	1.17e+9

Table 15
Estimated pitting service life of the sun gear in regard to different R.

Item	Position	Case 3			
		105 (%) R	N_p	115 (%) R	N_p
Sun gear	p1	0.0293	1.94e+9	0.0321	2.36e+9
	0	0.0285	1.42e+9	0.0311	1.74e+9
	m1	0.0218	9.99e+8	0.0239	1.22e+9

age are limited for the four cases considered in this study, which will increase with increasing U_m.

5. Conclusions

In this study, a time domain-based gear contact fatigue analysis of NREL's 750 kW land-based Gearbox Reliability Collaborative wind turbine is performed. The main purpose is to investigate how the long-term distribution of gear contact pressures can be represented by analytical functions such as the Weibull distribution and the generalized gamma distribution. These distributions are necessary for the reliability-based design of gears using probabilistic approaches and to develop simplified methods for practical design. The main conclusions from the study are as follows:

(I) A new simplified predictive subsurface pitting model to estimate the service lives of gears under dynamic conditions is presented. The applicability of the model is verified by comparing the results with published experimental evidence. It could be also used for more advanced gearbox models, where the gear tooth contact forces need to be recalculated.
(II) The decoupled analysis method is used for the dynamic analysis of the gears in the drive-train system of the wind turbine and is verified by comparing the results with those from a fully-coupled dynamic analysis of the wind turbine with the gearbox model.
(III) The two-parameter Weibull function, the generalized gamma function and the three-parameter Weibull function can be used to fit the long-term probability distribution of the gear contact pressures under dynamic conditions. The generalized gamma function is better than the other functions, and the two-parameter Weibull function is simpler than the others.
(IV) Based on the gear models used in this study, the sun gear is more critical than the planet gear in terms of pitting. The critical locations for the sun gear and the planet gears are in their recess areas; this is because the equivalent radius R near the recess contact point is much smaller than the pitch and the engagement contact points, which leads to a larger equivalent maximum contact pressure range $\Delta\bar{p}_{\max}$.
(V) A so-called 'limit state function' for reliability-based probabilistic contact fatigue analysis could be established based on the pitting life prediction model presented in this paper; this will be performed in future work. In addition, the model could also be used to check gear designs for different wind farms, especially for different offshore sites where the environmental conditions vary significantly.

This study only considers the torque loads in the main shaft under normal operating conditions. The effects of non-torque loading should be investigated in future work. In addition, other operational loads, e.g. excitations from generator side to the gearbox and the transient loading, should be also considered in fatigue analysis in future work. Furthermore, time-domain simulations of larger megawatt wind turbines (onshore and offshore) should be performed. In this paper, only subsurface pitting is considered. Other failure modes of gears (e.g., high cycle bending fatigue, wear, scuffing et al. [61]) could also be investigated in a similar way, where the main challenge is to obtain predictive physical failure models.

Acknowledgements

The authors wish to acknowledge the support from the Research Council of Norway through the Centre for Ships and Ocean Structures at the Norwegian University of Science and Technology in Trondheim, Norway. The gearbox and wind turbine model is obtained with courtesy from the Gearbox Reliability Collaborative (GRC) project at the National Renewable Energy Laboratory, Colorado, USA. The GRC initiative is funded by the Wind and Water Power Program of the United Stated Department of Energy. In addition, the authors also wish to acknowledge the explanation and instruction from Dr. Osman, T. for their contact fatigue prediction model, who is from the Contact and Structural Mechanics Laboratory (LaMCoS) in National Institute of Applied Sciences in Lyon (INSA Lyon).

References

[1] McNiff B, Musical WD, Errichello R. Variations in gear fatigue life for different wind turbine braking strategies. Golden, Colorado USA: Solar Energy Research Institute; 1990.

[2] ISO/IEC 81400-4. Wind turbines-part 4: standard for design and specification of gearboxes. The international organization for standardization: Geneva, Switzerland; 2005.
[3] AGMA standard 2003-A86. AGMA standard for rating the pitting resistance and bending strength of spur and helical involute gear teeth; 1982.
[4] DIN (Deutsche Institut fur Normung) 3990. Tragfahigkeits-berechnung von Stirnradern. Beuth Verlag GMBH; 1987.
[5] ISO standard 6336-2. Calculation of load capacity of spur and helical gears – part 2: calculation of surface durability (pitting). The international organization for standardization: Geneva, Switzerland; 2006.
[6] Glodez S, Flasker J, Ren Z. A new model for the numerical determination of pitting resistance of gear teeth flanks. Fatigue Fract Eng Mater Struct 1997;20(1):71–83.
[7] Way S. Pitting due to rolling contact. ASME J Appl Mech 1935;2:A49–58.
[8] Coy JJ, Townsend DP, Zaretsky EV. Dynamic capacity and surface fatigue life for spur and helical gears. ASME J Lubr Technol 1976;98:267–76.
[9] Lundberg G, Palmgren A. Dynamic capacity of roller bearings. ACTA Polytechnica Mech Eng Ser 1952;2(4).
[10] Keer LM, Bryant MD, Haritos GK. Subsurface and surface cracking due to hertzian contact. ASME J Lubr Technol 1982;104:347–51.
[11] Keer LM, Bryant MD. A pitting model for rolling contact fatigue. ASME J Lubr Technol 1983;105:198–205.
[12] Murakami Y, Kaneta M, Yatsuzuka H. Analysis of surface crack propagation in lubricated rolling contact. ASLE Tribol Trans 1985;28(1):60–8.
[13] Hanson MT, Keer LM. An analytical life prediction model for the crack propagation occurring in contact fatigue failure. ASLE Tribol Trans 1992;35(3):451–61.
[14] Mow VC, Cheng HS. The thermal stresses in an elastic half-space associated with an arbitrarily distributed fast-moving heat source. ASME J Basic Eng 1965;87:729–34.
[15] Goshima T, Hanson MT. Three-dimensional analysis of thermal effects on surface crack propagation in rolling contact. J Therm Stresses 1990;13(3):237–61.
[16] Glodez S, Winter H, Stuwe HP. A fracture mechanics model for the wear of gear flanks by pitting. Wear 1997;208:177–83.
[17] Glodez S, Potocnik R, Flasker J, Zafosnik B. Numerical modelling of crack path in the lubricated rolling–sliding contact problems. Eng Fract Mech 2008;75:880–91.
[18] Fajdiga G, Flasker J, Glodez S. The influence of different parameters on surface pitting of contacting mechanical elements. Eng Fract Mech 2004;71:747–58.
[19] Osman T, Velex Ph. A model for the simulation of the interactions between dynamic tooth loads and contact fatigue in spur gears. Tribol Int 2012;46(1):84–96.
[20] Jonkman JM, Marshall L, Buhl Jr. FAST user's guide. Technical Report NREL/EL-500-38230. National Renewable Energy Laboratory (NREL). Golden, Colorado, USA; 2005.
[21] SIMPACK Release 8.9. SIMPACK Reference Guide. SIMDOC v8.904. 2010.
[22] Cheng W, Cheng HS, Mura T, Keer LM. Micromechanics modeling of crack initiation under contact fatigue. ASME J Tribol 1994;116:2–8.
[23] Mura T, Nakasone Y. A theory of fatigue crack initiation in solids. ASME J Appl Mech 1990;57:1–6.
[24] Glodez S, Sraml M, Kramberger J. A computational model for determination of service life of gears. Int J Fatigue 2002;24:1013–20.
[25] Fajdiga G, Sraml M. Fatigue crack initiation and propagation under cyclic contact loading. Eng Fract Mech 2009;76:1320–35.
[26] Agha SR. Fatigue performance of superfinish hard turned surfaces in rolling contact. Purdue University. PhD thesis; 2000.
[27] Jiang B, Zheng X, Wang M. Calculation for rolling contact fatigue life and strength of case-hardened gear materials by computer. J Test Eval 1993;21(1):9–13.
[28] Fleming JR, Suh NP. The relationship between crack propagation rates and wear rates. Wear 1977;44:57–64.
[29] Choi Y, Liu CR. Rolling contact fatigue life of finish hard machined surfaces part 1. Model development. Wear 2006;261:485–91.
[30] Chen Q, Leng X, Shao E. Influence of microstructure and residual stress on the stages of case crushing. Wear 1988;122:45–55.
[31] Hearle AD, Johnson KL. Mode II stress intensity factors for a crack parallel to the surface of an elastic half-space subjected to a moving point load. J Mech Phys Solids 1985;33(1):61–81.
[32] Choi Y, Liu CR. Rolling contact fatigue life of finish hard machined surfaces, part 2. Experimental verification. Wear 2006;261:492–9.
[33] Straffilini G, Marcu Puscas T, Molinari A. Identification of rolling–sliding damage mechanisms in porous alloys. Metall Mater Trans 2000;31:3091–9.
[35] Smith JO, Liu CK. Stresses due to tangential and normal loads on an elastic solid with application to some contact stress problems. ASME J Appl Mech 1953;20:157–66.
[36] Lang OR. Dimensioning of complicated steel machine part in the whole range of load cycle and endurance. Materialwiss Werkstofftech 1979;10:24–9 [in German].
[37] Tobe T, Kato M, Inoue K. Bending strength of carburized SCM42OH spur gear teeth. Bull JSME 1986;29:273–80.
[38] Kato M, Deng G, Inoue K, Takatsu N. Evaluation of the strength of carburized spur gear teeth based on fracture mechanics. J Soc Mech Eng Int J Ser C 1993;36:233–40.
[39] Melchers RE. Structural reliability analysis and prediction. 2nd ed. John Wiley & Sons Ltd.; 2002.
[40] Hobn BR, Michaelis K, Vollmer T. Thermal rating of gear drives: balance between power loss and heat dissipation. AGMA Technical Paper 1996. ISBN: 1-55589-675-8.
[41] Martins R, Seabra J, Brito A, Seyfert Ch, Luther R, Igartua A. Friction coefficient in FZG gears lubricated with industrial gear oils: biodegradable ester vs. mineral oil. Tribol Int 2006;39:512–21.
[42] Leng X, Chen Q, Shao E. Initiation and propagation of case crushing cracks in rolling contact fatigue. Wear 1988;122:33–43.
[43] Govindarajan N, Gnanamoorthy R. Rolling/sliding contact fatigue life predication of sintered and hardened steels. Wear 2007;262:70–8.
[44] Bir GS, Oyague F. Estimation of blade and tower properties for the gearbox research collaborative wind turbine. Technical Report NREL/EL-500-42250. National Renewable Energy Laboratory (NREL). Golden, Colorado, USA; 2007.
[45] Oyague F. GRC Drive Train Round Robin GRC 750/48.2 Loading Document (IEC 61400-1 Class IIB). Golden, Colorado, USA; 2009.
[46] Kaimal JC, Wyngaard JC, Izumi Y, Cote OR. Spectral characteristics of surface-layer turbulence. Q J R Meteorol Soc 1972;98:563–98.
[47] International Standard IEC-61400-1. Wind turbines. Part 1: design requirements. 3rd ed. International electrotechnical commission. Geneva, Switzerland; 2005.
[48] Dong WB, Xing YH, Moan T. Time domain modeling and analysis of dynamic gear contact force in wind turbine gearbox with respect to fatigue assessment. Energies 2012;5(11):4350–71.
[49] ISO Standard 6336-1. Calculation of load capacity of spur and helical gears – Part 1: basic principles, introduction and general influence factors. 2nd ed. The international organization for standardization: Geneva, Switzerland; 2006.
[50] Flodin A, Andersson S. A simplified model for wear prediction in helical gears. Wear 2001;241:285–92.
[51] Xing YH, Karimirad M, Moan T. Modeling and analysis of spar-type floating wind turbine drivetrain. Wind Energy; submitted for publication.
[52] Xing YH, Moan T. Multi-body modeling and analysis of a planet carrier in a wind turbine gearbox. Wind Energy; accepted for publication.
[53] Nejad AR, Xing YH, Moan, T. Gear train dynamics in large offshore wind turbines. The ASME 2012 11th Biennial Conference on Engineering Systems Design and Analysis, Nantes, France; 2012.
[54] LaCava W, Xing YH, Guo Y, Moan T. Determining wind turbine gearbox model complexity using measurement validation and cost comparison. Copenhagen, Denmark: European Wind Energy Association Annual Event; 2012.
[55] Xing YH, Karimirad M, Moan T. Effect of spar-type floating wind turbine nacelle motion on drivetrain dynamics. Copenhagen, Denmark: European Wind Energy Association Annual Event; 2012.
[56] Kiss P, Janosi IM. Comprehensive empirical analysis of ERA-40 surface wind speed distribution over Europe. Energy Convers Manage 2007;49(8):2142–51.
[57] Uppala SM, Kallberg PW, Simmons AJ, Andræ U, Da costa Bechtold U, Fiorino M, et al. The ERA-40 re-analysis. Q J R Meteorol Soc 2005;131:2961–3012.
[58] Hoogwijk M, De Vries B, Turkenburg W. Assessment of the global and regional geographical, technical and economic potential of onshore wind energy. Energy Economics 2004;26:889–919.
[59] New M, Hulme M, Jones P. A 1961–1990 mean monthly climatology of global land areas. Norwich: Climate Research Unit; 1997.
[60] New M, Hulme M, Jones P. Representing twentieth century space-time climate variability: part I. Development of a 1961–1991 mean monthly terrestrial climatology. American Meteorological Society; 1999. p. 820–56.
[61] Sheng SW, McDade M, Errichello R. Wind turbine gearbox failure modes – a brief. ASME/STLE 2011 International Joint Tribology Conference, Los Angeles, California; 2011.